Investigation of stress field with neutron diffraction of welds based on a temper bead technique.

Romain Jeanpierre, Sébastien Rouquette, Dominique Deveaux, Frédéric Deschaux-Beaume, Laurent Jubin, Fabien Soulié, Fabien Lefebvre

77th IIW Annual Assembly and International Conference on Welding and Joining 7-12 July 2024 Rhodes, Greece

Investigation of stress field with neutron diffraction of welds based on a temper bead technique.

Romain JEANPIERRE[12], Sébastien ROUQUETTE[1], Dominique DEVEAUX[2], Frédéric DESCHAUX-BEAUME[1], Laurent JUBIN[2], Fabien SOULIÉ[1], Fabien LEFEBVRE[2]*

[1]LMGC, Univ. Montpellier, CNRS, Montpellier, France
[2]CETIM, 52 Avenue Félix Louat,60304 Senlis, France
* corresponding author: romain.jeanpierre@cetim.fr

Abstract. Residual stress is a well-known consequence of welding which may promote cold cracking, stress-corrosion cracking, or fatigue cracks growth phenomena of steel pressure vessels. Residual stresses can be reduced by post weld heat treatment (PWHT). However, such treatments may not be usable on-site for welding repair of pressure vessels. "Temper bead welding" (TBW) techniques have been developed and introduced as substitution to PWHT for steel structures in construction codes because of their abilities to temper or to refine the heat affected zone (HAZ). Then TBW techniques reduce cracking risks related to the initial presence of brittle or hard metallurgical phases in the HAZ of steels. Nevertheless, reduction of residual stresses is not clearly made evident with TBW techniques. In this context, residual stresses induced by deposition of weld beads following a TBW technique were investigated with neutron diffraction carried out at SINQ instrument, Villigen, Switzerland. This communication describes the experiment and the resulting evolution of residual stresses up to five adjacent beads deposited on the surface of 20 mm thick P355 NH steel plates. The results show that the zone under tensile stress along longitudinal direction expands. For the five plates, the peak of transverse stress is equal to half of the maximal longitudinal stress.

1 Introduction

During arc-welding operation, the heat input, which allows the metal to melt and thereby forms the weld joint, also conducts to high thermal gradients around the bead during welding. Consequently, complex residual stress field appears after welding, mainly due to the non-uniform strain field induced by thermal dilatation and contraction according to the various thermal cycles reached in each zone around the deposited bead. Residual stresses may reach values close to the yield strength of the material. For a well-known configuration as a butt weld of carbon steel plates, the longitudinal stress field, i.e. along the direction parallel to the bead, generally shows high tensile stresses in the weld zone and heat affected zone, and compressive stresses elsewhere [1–3]. However, the stresses distribution depends on the thermal, metallurgical, and mechanical properties of the base and filler metals. For example, the use of a low temperature transformation filler metal could lead to compressive stresses in the weld bead by the formation of martensite at low temperature range [4,5]. Besides the materials properties, the parts design also influences the final level of residual stresses, depending on the global stiffness of the structure. Thin plates easily accommodate the thermal shrinkage during cooling after welding leading to a low residual stresses level, while on the opposite, thicker plates, or pipes, by a self-restrained effect, deform less but generate more residual stresses [6–8].

In power plant components, residual stresses are well known to contribute to many damage phenomena. High residual stresses could lead to reduction of their lifetime by increasing the fatigue crack propagation, by promoting cold cracking or even by stress-corrosion cracking [9–11]. Post-weld heat treatments (PWHT) are used to reduce residual stresses by achieving stress relieving with generation of creep strain and plastic deformation [12]. However, PWHT needs to heat the component up to 500 to 600 °C during several hours, depending on its composition and size, which, in the case of in-situ maintenance and repair, may be time-consuming, expensive, or potentially unadvisable. To solve these shortcomings, an alternative to PWHT has been developed, namely temper-bead welding techniques (TBW) [13,14].

The temper bead welding techniques are multipass welding operations in which the heat input, the welding parameters and the location of each bead have been precisely chosen to generate a tempering and/or a refinement effect in the heat affected zones (HAZ) created by the deposition of the first beads. These techniques commonly consist in deposing several layers of different heat input levels. The first layer, i.e. the one directly deposited on the base metal, has a low energy level in order to produce a thin HAZ, which will be thermally re-affected by the second layer deposition, by refinement or tempering, and by the third one, by tempering [15–17]. There are several TBW techniques, which differ mainly on the targeted metallurgical transformation. Using low alloy steels, the TBW techniques have showed their ability to effectively reduce the maximal hardness level, to produce a soft and thin microstructure or to maximize the impact toughness of the HAZ. Which finally lead them to be used as

substitutes for PWHT in the construction and repair codes, under very specific conditions.

Nevertheless, the main use of PWHT is to relieve residual stresses. So even if TBW techniques could affect metallurgical microstructure as PWHT, in such a manner that they reduce cracking risks linked with the presence of brittle, hard or coarse phases in the HAZ, it is still needed to understand if TBW techniques affect the residual stresses field before proposing them as fully valid alternatives to PWHT. As presented in [4,5], metallurgical transformations have an influence on the residual stresses, this may be the way for a TBW procedure to affect them.

This work presents the investigation of residual stresses evolution induced by consecutive deposition of the five first weld beads constituting the first layer of a TBW procedure. Residual stresses were characterized with neutron diffraction technique.

2 Welding procedure specifications

The material used for this study is made of a carbon steel grade EN 10028-3 P355NL commonly used in the fabrication of pressure vessels. The chemical composition of the filler metal and base metal are given in Table 1. The plates dimensions are 300 mm x 100 mm x 20 mm.

Four different weld configurations were carried out. They consist in deposing 1,3,4 or 5 beads on the top surface of each plate, like described in the **Fig. *1***. The first bead was systematically deposited at 40 mm from the left edge of the plate. Thus the 5 beads were centered in the middle of the plate. The weld beads were 220 mm long with start and stop position at 40 mm from each extremity of the plates. They were produced with the flux cored arc welding process (FCAW) coupled with Ar-18% CO_2 protection gas and rutile flux cored wire of 1.2 mm diameter. The plates were clamped during all the welding operation including several hours after cooling down to room temperature. The welding parameters used for the various beads are given in **Table 2**. In the case of multiple beads configurations, the inter-pass temperature was about 40-50 °C and the overlapping between adjacent beads was a bit less than 50%.

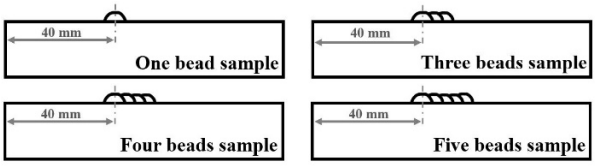

Fig. 1. Illustration of the samples cross sections.

3 Neutron diffraction measurements

Neutron diffraction technique allows the residual stresses measurements by a non-destructive way into thick components. By using the Bragg's law, mentioned in equation (1), it is possible to determine elastic strain by comparing the atomic lattice spacing d_{hkl} of the crystallographic plan *hkl* subjected to stresses with the stress-free spacing d_0 of this same plan, as mentioned in the equation (2). At constant wavelength λ and under tensile stress, the lattice spacing d_{hkl} will growth, leading to a shift toward lower value of the peak position θ_{hkl}, and inversely, compressive stress will bring a higher peak position θ.

$$2\, d\, sin(\theta) = n\, \lambda \tag{1}$$

$$\varepsilon_{hkl} = \frac{d_{hkl} - d_0}{d_0} \tag{2}$$

Where, *hkl* correspond to the Miller indices of the crystallographic plan of interest.

Once the elastic strains are measured along the three main directions of the plates samples, it is possible to compute the stresses along those directions by using generalized Hooke's law as below, in equation (3):

$$\sigma_i = \frac{E_{hkl}}{1+\nu}\varepsilon_i + \frac{\nu E_{hkl}}{(1+\nu)(1-2\nu)}\sum_{i=1}^{3}\varepsilon_i \tag{3}$$

Where E_{hkl} and ν are respectively the Young's modulus and the Poisson's ratio of the plan *hkl*, *i* corresponds to one of the direction *X, Y* or *Z*, i.e in our case, the longitudinal, transversal, and normal ones in the plates coordinate system, as represented in **Fig. 2**. Neutron diffraction technique was used with the diffractometer POLDI of the Paul Scherrer Institute (PSI), Villigen, Switzerland. It uses time-of-flight technique with thermal neutrons produced by the spallation source SINQ and allows the acquisition of a wide diffraction pattern permitting the observation of several diffraction peaks [18].

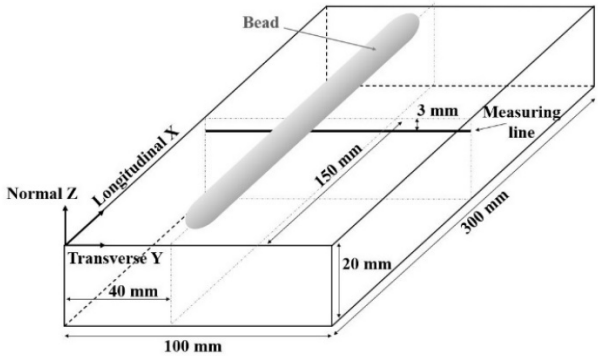

Fig. 2. Schematic representation of the coordinates system, of the plate dimensions and of the measuring line.

Table 1. Chemical compositions (in wt. %)

Elements	C	Si	Mn	P	S	N	Al	Cu	Cr	Ni	Mo	V	Ti	Nb	Fe
Base metal	0.16	0.2	1.47	0.016	0.002	0.004	0.041	0.04	0.05	0.04	0.01	0.001	0.002	0.02	Balance
Filler metal	0.05	0.47	1.23	0.015	0.011	-	< 0.1	0.09	0.03	0.02	< 0.01	0.02	-	< 0.01	

Table 2. Welding parameters used for the bead depositions

Weld bead	Arc voltage (V)	Wire feed speed (m/min)	Welding current (A)	Welding speed (cm/min)	Contact tip distance (mm)	Travel angle (°)	Work angle (°)
1	26.0	4.5	160 - 165	45	15	5 (push)	0
2 - 5				40		0	85

The strains in the 3 directions were measured along a line parallel to the surface in the middle-transverse section of each plate, at a depth of 3 mm under the surface on which the beads have been deposited, as shown in the **Fig. 2**. 12 to 14 points of measurements have been performed depending on the sample. The stress/strain-free sample (or d_0 sample) consisted of "comb-like" specimens. They were produced with wire electrical discharge machining (WEDM) by cutting a transverse slice of 4 mm thick taken in specimens produced in the same manner as the one used for residual stresses measurement. Grooves have then been cut all along the slices, as show in the **Fig. 3**.

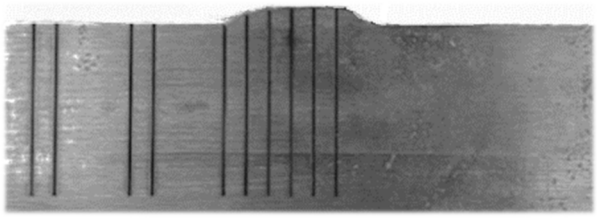

Fig. 3. Typical "comb-like" specimen with 5 beads

During the experiments, the detector centre was positioned at a scattering angle 2θ = 90°. A gauge volume of 3.8 x 3.8 x 3.8 mm^3 was used for the measurements along the longitudinal direction of the plates, and 3.8 x 3.8 x 10.0 mm^3 for the transversal and normal directions. A schematic illustration of the gauge volume plotted on the cross-sectional macrograph of the 5 beads specimen is shown **Fig. 4**.

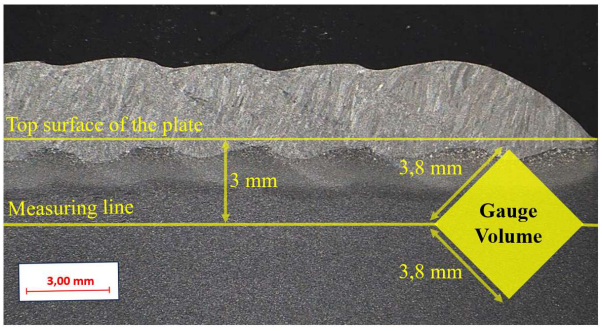

Fig. 4. Cross-sectional macrograph of the five beads specimen with an illustration of the gauge volume size

The data were post-processed with Mantid software [19]. The treatment has been conducted on the diffraction peak associated with the BCC crystallographic plane (211) of the P355NL steel, because of its stress-strain response. The Young's modulus and the Poisson's ratio have respectively been taken equal to 212.5 GPa and to 0.32.

The fitting process chosen in Mantid allows to work directly on the lattice constant a, which is linked to the lattice spacing of a cubic structure d with equation (4). The reference lattice constant, a_0, was chosen equal to 2.86651 Å.

$$\frac{1}{d^2} = \frac{h^2 + k^2 + l^2}{a^2} \quad (4)$$

4 Results and discussion

An example of a typical diffraction spectrum obtained during the experiment is shown in Fig. **5**. It represents the peak intensity vs. the scattering angle, each peak corresponding to a specific crystallographic plane on which the neutrons diffracted. The fitted curve, in dot line, is also illustrated and was used to get micro strains and then, residual stresses.

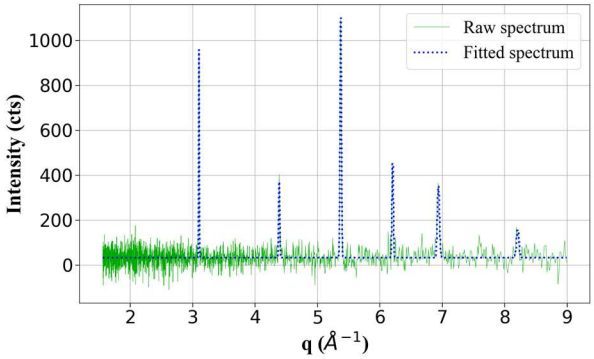

Fig. 5. An example of a neutron diffraction spectrum obtained in one point: experimental data (green line) and fitted one (blue dot line)

Fig. **6** and Fig. **7** show the stress distribution in samples with one and five beads along the three main directions. Based on the uncertainty in the peak diffraction position, the error bars are shown on the plotted figures. They reach a maximal value of +/- 60 MPa, below the welds because of the thickness of the beads, while in the base metal the uncertainties are around +/- 30 MPa.

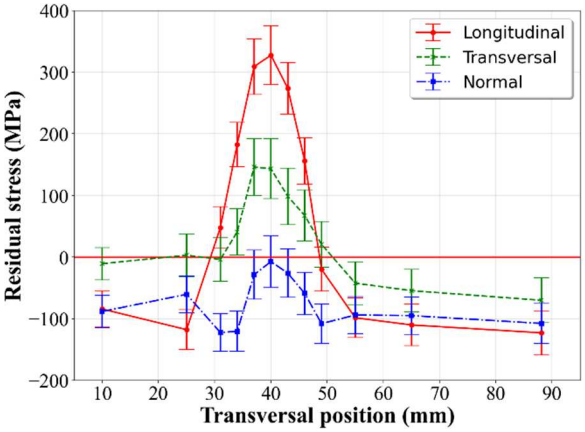

Fig. 6. Residual stresses in the sample with one bead

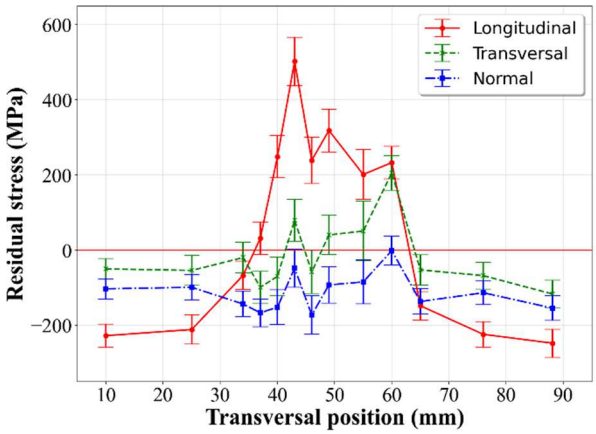

Fig. 7. Residual stresses in the sample with five beads

The sample with one bead shows that the longitudinal residual stress, σ_{LD}, reaches a maximal value of 330 MPa at a location just under the bead center. As expected, tensile longitudinal stresses are generated below the weld zone, surrounded by a zone under compressive longitudinal stresses. The maximal stress value rises to 500 MPa with the five beads specimen, which is 90 MPa higher than the yield strength of the base metal. Let us point out that the stresses measured by the diffraction technique are averaged through the gauge volume, so we can expect that, at a smaller scale, the maximal level of residual stress may end up well above the yield strength.

Fig. ***8***, Fig. ***9*** and Fig. ***10*** show respectively the evolution of the longitudinal, transverse, and normal stresses, respectively σ_{LD}, σ_{TD}, and σ_{ND}, along the transverse axis following the successive deposition of the 1st, 3rd, 4th and 5th bead. For clarity, the uncertainty bars are only plotted on the 5 beads configurations, where they are the highest, and the transversal positions of the centre of 1st, 3rd, 4th and 5th beads are represented by vertical green lines.

Regarding σ_{LD} , the zone under tensile stress expands mainly to the right as presented in **Fig. *8*** where the beads are newly deposited. The maximal tensile value rise from 330 MPa, for the first bead, to 480 MPa at the 3rd one.

Surprisingly, the maximum value reached after the 4th weld bead is located between the centre of the 1st and 3rd weld bead, and not below the centre of the 4th bead, as expected. This value reaches 570 MPa. The lowest σ_{LD} values are also reached after the 4th weld bead, on either side of the area where the beads were deposited, at transversal positions 25 mm and 65 mm, with a value close to -290 MPa.

For the plates with 3, 4 and 5 beads, the profiles of longitudinal stress consist in a tensile stress peak next to a plateau of around half or two third of the value reach by the peak. This area is then surrounded by compressive stresses zone where the intensity is almost equal to the one reached in the plateau area.

Concerning σ_{TD} distributions presented in **Fig. *9***, the maximum value is located close to the centre of the last deposited weld bead. The width of the tensile zone is slightly reduced after 3rd, 4th and 5th bead in comparison to the 1st bead. Most of the sample exhibit compressive transverse stress except under the last deposited weld bead.

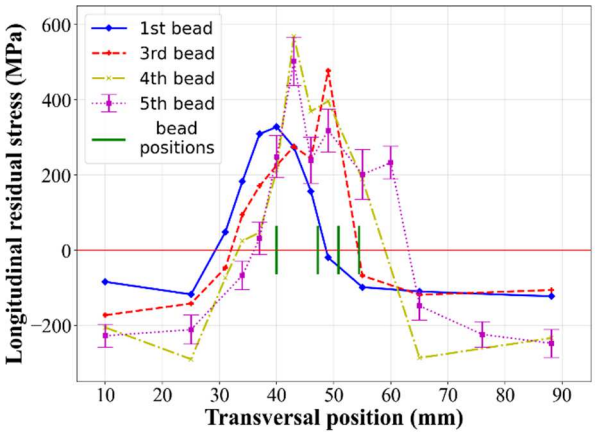

Fig. 8. Longitudinal stresses measured on the 4 configurations.

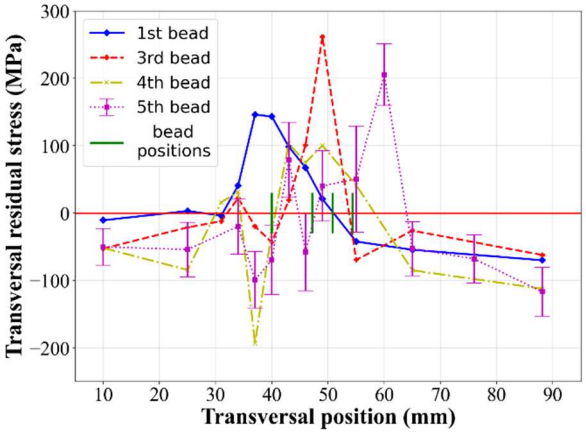

Fig. 9. Transversal stresses measured on the 4 configurations.

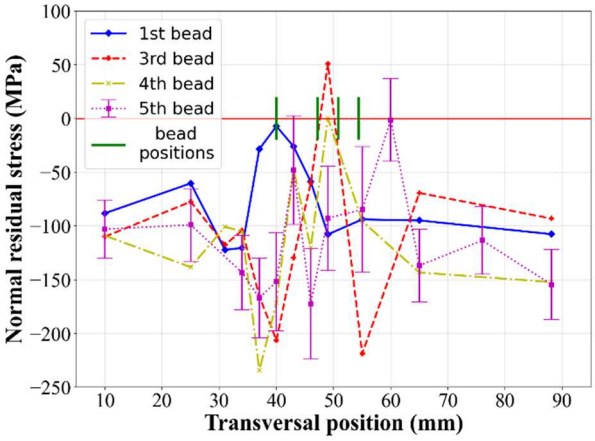

Fig. 10. Normal stresses measured on the 4 configurations.

The normal stress distributions are presented in **Fig. *10*** for all studied samples. These distributions are almost compressive and varying around a constant value of -100 MPa. σ_{ND} show a wavy behaviour in the zone below the weld beads. It varies between a maximum value of 50 MPa, observed in the three beads plate, to a minimum value of -215 MPa.

As described previously, the residual stresses distributions measured in the one bead specimen is close to the ones found in the literature. Directly under the bead, σ_{LD} and σ_{TD} are tensile stresses with respectively a

peak of 330 MPa and 150 MPa, while elsewhere low stress or compressive stresses area are found. This typical shape is explained by the simultaneous rise of the elastic stiffness of the bead area and its shrinkage under self-restraint condition during cooling to ambient temperature [1,2].

Concerning σ_{TD}, the global strain incompatibility created by the contraction and the restraint of the bead area is less intense than the one involved along the longitudinal direction, conducting to lower stress values. A clear asymmetry is visible around the tensile area leading, on the left side of the peak, to a region where the stresses are close to 0, while on the right region the compressive stresses reach -70 MPa. This asymmetric distribution may be explained by the off-centre deposition of the first bead and by the restraint during welding, the influence of the latter having been evaluated in [8].

While the normal stress, σ_{ND}, is fully compressive, a low stress value is measured under the bead. The normal stress distribution shows a similar shape than the transversal direction: higher stress values below the bead location surrounded by compressive stress region with an asymmetric distribution. However, in this direction, the higher stress value reaches almost 0 MPa, while on the right side it reaches -100 MPa, and on the left side it shows a compressive peak of -120 MPa followed by a rise to -80 MPa. This compressive stress state could be explained by the formation of martensite during the colling of the bead and the HAZ, leading to a volume expansion, and as previously explained, by the off-centre deposition and by the auto-restraint effect.

After the deposition of the 3rd bead and when compared to the previous stress distributions, the peak of σ_{LD} stress initially present below the first bead move to the right, from y = 40 mm to y = 48 mm, and rose from 330 MPa to 480 MPa. This peak translation is also accompanied with a local diminution of σ_{LD} below the first deposited bead and with an expansion on the right of the width of the area under tensile stress. The fused metal, produced by the deposition of the new bead, shrink during solidification and cooling what generates a new tensile stress zone below the new deposited bead which was added to the previous one, that explain the shift to the right of the σ_{LD} peak. The same mechanism may also explain the local reduction of σ_{LD} below the first bead: a new bead deposition also creates around the tensile stress zone a compressive zone that can reduce the initial tensile stress state.

The transversal stresses induced by the 3rd bead deposition led to the formation of compressive stress in place of the previous tensile peak under the first bead, driving a reduction of σ_{TD} from 150 to -40 MPa. In addition, a high tensile peak is formed under the 3rd bead location reaching 260 MPa. The normal stress distribution follows almost the same evolution than σ_{TD}: in place of the previous highest value, i.e. under the first bead, an intense reduction is observed, σ_{ND} goes from 0 MPa to -200 MPa, coupled with a shift of the previous highest value peak under the 3rd bead location. This new peak reaches 50 MPa and is surrounded by two narrow compressive zones reaching -220 MPa.

The reduction of the σ_{TD} and σ_{ND} stresses and the formation of a compressive zone below the first bead underline the creation of a compressive stress area sufficiently intense to totally reduce the tensile stress initially present before the 3rd bead deposition. Knowing that the effect on the residual stresses of the 3rd bead deposition should be almost the same than the one observed during the deposition of the 1st one, i.e. creations of tensile peak surrounded by compressive zones, it is likely that the compressive area induced by the deposition of the third bead have been superposed to the tensile zone created by the two previous beads, leading to lower residual stresses values. The metallurgical transformations induced in the HAZ of the 3rd bead could also lead to more intense and extensive compressive area if martensite is formed, as explained before and as suggested by the presence of σ_{TD} and σ_{ND} compression peaks in the base metal around the tensile area below the third bead.

The deposition of the 4th bead, as for the previous one, leads to a new reduction of σ_{LD} below the first bead on the left part, for transversal positions between 10 and 40 mm. However, a new reduction does not occur with the 5th bead deposition, maybe because the location of this latter is too far away to influence the stress state below the first bead. Concerning the 4 and 5 beads configurations, an expansion of the σ_{LD} tensile zone to the right side is again observed, likely following the same mechanism described in the case of the 3 beads sample. But contrary to what can be expected, the tensile peaks for σ_{LD} are not located below the last deposited bead, but on their left. This result could be explained by a possible transformation of the martensite formed during the previous deposits into ferrite, generating a volume shrinkage during the deposition of the 4th and 5th beads, producing an increase of tensile stresses on the left of the new deposited beads. In opposite, the area below the new deposited beads still benefits from the formation of martensite, leading to lower stresses.

Concerning σ_{TD} of the 4 and 5 beads specimens, and as for the 3 beads configuration, the tensile stresses area generated by the deposition of the new bead is surrounded by two compressive stress areas. As for the third bead sample, one can explain this result by the formation of martensite in the HAZ during the deposit.

The displacement phenomenon of the stress peak is also observed for the normal stress, σ_{ND}, where the stress peak move to the right, except for the 4 beads configuration. The transversal and normal stresses profiles for this sample are untypical, concerning the maximum stress and the location of the peak. This could be due to a too high gauge volume and to the location of the measure areas, that do not allow to measure the highest tensile stress value for this configuration.

Lastly, especially in the case of σ_{TD} and σ_{ND}, it is possible to observe a real decrease of residual stresses around the 1st deposited bead during the deposition of the other beads, with an evolution of the tensile stresses towards compressive stress states. However, the maximal value at the stress peak measured in each of the four configurations along those two directions, remains

between 150 and 250 MPa, and does not show any clear tendency of reducing. It's also interesting to observe that no wide area with high tensile stresses develop, in total opposite with the behaviour of σ_{LD}. Concerning the stresses σ_{ND} measured in all four samples, our results show almost exclusively compressive stress states, in opposite to [8]. Each configuration exhibit non negligible stress levels with at least -120 MPa for the one bead specimen to -230 MPa for the 4 bead one.

5 Conclusion

In this study, the residual stresses induced by the successive deposition of the five first beads following a first stage of temper-bead procedure have been investigated using POLDI diffractometer at the Paul Scherrer Institute. This experimental work can be summarized as follow:

- After the deposition of the third bead, the σ_{LD} peak exceeds the yield strength of base metal by up to 150 MPa.
- The width of the zone under tensile longitudinal stresses increases with the bead depositions.
- The σ_{TD} distribution shows a tensile peak below the deposited bead, which is systematically reduced by the deposition of a new bead, and can even lead to the formation of compressive stresses. A new stress peak is created below the new deposited bead, but these peak displacements do not induce any expansion of the tensile area, contrary to what is observed for the longitudinal stresses.
- The evolution of the stress distributions and the creation of compressive zones could be due to the martensite formation in the HAZ.

Future works will focus on the deposition of subsequent layers on the top of the previous ones to better understand the influence of a complete TBW procedure on the final distribution of residual stresses.

6 Acknowledgements

The authors are grateful to Florencia Malamud and Jan Capek for their help and assistance during the experiments on the POLDI diffractometer at PSI. The authors would also like to acknowledge the contributions of Charles Bonan during the specimen design and welding.

7 References

[1] Kou, S., 2003, *Welding Metallurgy*, Wiley-Interscience, Hoboken, N.J.

[2] Radaj, D., 1992, *Heat Effects of Welding: Temperature Field, Residual Stress, Distortion ; with 265 Figures*, Springer, Berlin.

[3] Nitschke-Pagel, T., and Wohlfahrt, H., 2002, "Residual Stresses in Welded Joints – Sources and Consequences," MSF, **404–407**, pp. 215–226.

[4] Jiang, W., Chen, W., Woo, W., Tu, S.-T., Zhang, X.-C., and Em, V., 2018, "Effects of Low-Temperature Transformation and Transformation-Induced Plasticity on Weld Residual Stresses: Numerical Study and Neutron Diffraction Measurement," Materials & Design, **147**, pp. 65–79.

[5] Sun, J., Nitschke-Pagel, T., and Dilger, K., 2023, "Generation and Distribution Mechanism of Welding-Induced Residual Stresses," Journal of Materials Research and Technology, **27**, pp. 3936–3954.

[6] Leggatt, R. H., 2008, "Residual Stresses in Welded Structures," International Journal of Pressure Vessels and Piping, **85**(3), pp. 144–151.

[7] Park, J., An, G., Ma, N., and Kim, S., 2022, "Effect of Transverse Restraint on Welding Residual Stress in V-Groove Butt Welding," Metals, **12**(4), p. 654.

[8] Paradowska, A., Price, J. W. H., Ibrahim, R., and Finlayson, T., 2005, "A Neutron Diffraction Study of Residual Stress Due to Welding," Journal of Materials Processing Technology, **164–165**, pp. 1099–1105.

[9] Dong, P., and Brust, F. W., 2000, "Welding Residual Stresses and Effects on Fracture in Pressure Vessel and Piping Components: A Millennium Review and Beyond," Journal of Pressure Vessel Technology, **122**(3), pp. 329–338.

[10] Withers, P. J., 2007, "Residual Stress and Its Role in Failure," Rep. Prog. Phys., **70**(12), p. 2211.

[11] Kannengiesser, T., and Boellinghaus, T., 2013, "Cold Cracking Tests—an Overview of Present Technologies and Applications," Weld World, **57**(1), pp. 3–37.

[12] Dong, P., Song, S., and Zhang, J., 2014, "Analysis of Residual Stress Relief Mechanisms in Post-Weld Heat Treatment," International Journal of Pressure Vessels and Piping, **122**, pp. 6–14.

[13] Aloraier, A. et Al., 2010, "Weld Repair Practices without Post Weld Heat Treatment for Ferritic Alloys and Their Consequences on Residual Stresses: A Review," International Journal of Pressure Vessels and Piping, **87**(4), pp. 127–133.

[14] Doty, W. D., 1996, "History and Need behind the New NBIC Rules on Weld Repair without PWHT," Bulletin - Welding Research Council, (412).

[15] WTIA, 2006, *Temper Bead Welding*, TGN-PE-02, Welding Technology Institute of Australia.

[16] Lau, T. W., Lau, M. L., and Poon, G. C., 1996, "Development of Controlled Deposition Repair Welding Procedures at Ontario Hydro," Bulletin - Welding Research Council, (412).

[17] Wang, Y., Lundin, C. D., Qiao, C. Y. P., Khan, K. K., Al-Ejel, K., and Batten, G. W., 2005, *Half-Bead Temper-Bead Controlled Deposition Techniques for Improvement of Fabrication and Service Performance of Cr-Mo Steels*, Welding Research Council.

[18] Stuhr, U.et al., 2005, "Time-of-Flight Diffraction with Multiple Frame Overlap Part II: The Strain Scanner POLDI at PSI," Nuclear Instruments and Methods in Physics Research Section A: Accelerators, Spectrometers, Detectors and Associated Equipment, **545**(1), pp. 330–338.

[19] Arnold, O. et al., 2014, "Mantid—Data Analysis and Visualization Package for Neutron Scattering μ SR Experiments," Nuclear Instruments and Methods in Physics Research Section A: Accelerators, Spectrometers, Detectors and Associated Equipment, **764**, pp. 156–166.